SPE 141973

A Sparse Basis POD for Model Reduction of Multiphase Compressible Flow

S. Krogstad/SINTEF ICT

This paper was prepared for presentation at the 2011 SPE Reservoir Simulation Symposium held in The Woodlands, Texas, USA., 21–23 February 2011.

Abstract

We develop a sparse basis model-order reduction technique for approximation of flux/pressure fields based on local proper orthogonal decompositions (PODs) *glued* together using the Multiscale Mixed FEM (MsMFEM) framework on a coarse grid. Based on snapshots from one or more simulation run, we perform singular value decompositions (SVDs) for the flux distribution over coarse grid interfaces and use the singular vectors corresponding the largest singular values as boundary conditions for the multiscale flux basis functions. The span of these basis functions matches (to prescribed accuracy) the span of the snapshots over coarse grid faces. Accordingly, the complementary span (what's left) can be approximated by local PODs on each coarse block giving a second set of local/sparse basis functions. The reduced system unknowns corresponding to the second set of basis functions can be eliminated to keep the system size low.

To assess the accuracy, we apply the methodology to two test problems (including compressibility and gravity) and compare to results obtained from full order simulations. The methodology produces accurate results for a large variation of coarse grids, but we do observe that a large number of basis vectors are needed where the flow is strongly dominated by gravity.

Compared to standard POD, the suggested sparse version results in a larger number of basis functions, but requires overall less storage. Also the sparse POD appears to be more process independent. An additional benefit is that SVDs are performed on multiple *small* matrices rather than on one *big*.

Introduction

The ability to perform fast reservoir simulation is crucial for optimization workflows within real-time/closed-loop reservoir management. Current simulators are far from meeting these requirements if detailed geological information is to be utilized, so reducing the order of the models become inevitable. Reduced order modeling techniques using proper orthogonal decompositions (POD) have recently received interest in reservoir simulation research (see e.g., van Doren et al. (2006), Cardoso et al. (2008), and references therein). On the other hand, much effort has been put into accurate coarse discretizations using multiscale methods. Common for these techniques is that they seek efficient solutions of equations with rough coefficients without scale separation through the use of numerically computed basis functions. Locally computed multiscale basis functions may suffer from resonance errors, and a way to overcome this is through the use of global information in setting the boundary conditions for the bases (see e.g., Aarnes et al. (2006); Effendiev et al. (2006); Aarnes et al. (2008)). Using global information in the computation of multiscale basis functions produce accurate results for incompressible flow, but for strong compressibility and gravitational forces, accurate boundary conditions may be insufficient. To this end local correction functions were introduced in Lunati and Jenny (2006) and later by Krogstad et al. (2009).

In this work we combine some of the POD-based reduced order modeling techniques with multiscale mixed-finite-element (MsMFE) basis functions to produce a sparse/localized reduced order basis for compressible flow problems. The paper proceeds as follows: we start by introducing the fine-grid discretization of the model problem before we introduce the reduced order (multiscale-type) bases, and finally we demonstrate the suggested methodology in two numerical examples. The first is a compressibility driven 2D problem, while the second problem is strongly influenced by gravity. Although simple, the examples illustrate that localized reduced order models may be more process independent than the global versions, and even though the number of basis vectors become larger, the increased sparsity reduces the storage requirements.

Model and Fine-Scale Discretization

We consider the equations for compressible three-phase flow in porous media for which capillarity is neglected. For simplicity, we only consider immiscible flow. The governing equations are the standard mass-conservation equations of the three phases

inside a computational domain Ω with boundary $\partial\Omega$,

$$\frac{\partial(\phi b_\ell s_\ell)}{\partial t} + \nabla \cdot (b_\ell \vec{u}_\ell) = q_\ell, \qquad \vec{u}_\ell = -\lambda_\ell \mathbf{K} \nabla p \text{ in } \Omega, \tag{1}$$

where $\ell = o, w, g$ denotes the three phases, ϕ is the porosity, b_ℓ is the inverse of the phase formation volume factor (ratio of density at reservoir condition to density at surface conditions), s_ℓ is the phase saturation, $\vec{u}_\ell$ is the phase volumetric flux (at reservoir conditions), q_ℓ is the source term, $\mathbf{K}$ is the absolute permeability, $\lambda_\ell = k_{r\ell}/\mu_\ell$ is the phase mobility, where $k_{r\ell}$ is the relative permeability and μ_ℓ is the phase viscosity.

In the following we assume that Eq. 1 is solved using an operator splitting method in which the flow and transport problems are solved separately, using an IMPES-like method or the sequential fully-implicit method (Tchelepi et al. 2007). To derive the pressure equation, we multiply the first equation in Eq. 1 by b_ℓ^{-1}, use the chain rule and sum over all three phases to eliminate saturation. We then insert the expression for the Darcy velocities and eliminate ∇p to give an equation of the form

$$c_t \frac{\partial p}{\partial t} + \nabla \cdot \vec{u} - (\zeta \vec{u} + \beta \mathbf{K} \vec{g}) \cdot ((\lambda \mathbf{K})^{-1} \vec{u} + \omega \vec{g}). \tag{2}$$

Here, $\vec{u} = -\lambda \mathbf{K}(\nabla p - \rho g \vec{e}_z)$ is the total Darcy velocity, where $\lambda = \sum \lambda_\ell$ is the total mobility; $\zeta = \zeta(s, p)$ is shorthand for $\sum c_\ell f_\ell$, where $f_\ell = \lambda^{-1}\lambda_\ell$ is the fractional flow function, $\omega = \sum \rho_\ell f_\ell$ and $\beta = \sum c_\ell \lambda_\ell (\omega - \rho_\ell)$; $q = \sum q_\ell / b_\ell$ is the total source; and c_ℓ and c_t are the phase and total compressibilities,

$$c_\ell = \frac{d \ln b_\ell}{dp}, \qquad c_t = \frac{d\phi}{dp} + \phi \sum_\ell c_\ell s_\ell. \tag{3}$$

Wells are considered as boundary conditions; that is, a well w with boundary Γ_w is conceptually represented as a *hole* in Ω with $\Gamma_w \subset \partial\Omega$, see Skaflestad and Krogstad (2008) for more details. Hence, Eq. 2 can be considered as free of source terms. In the following, we consider wells that are either pressure constrained ($p = p^w$ on γ_w) or rate constrained ($\int_{\gamma_w} \vec{u} \cdot \vec{n} = -q_w$ on Γ_w).

Discretization. We start by assuming that the computational domain Ω is represented by a grid consisting of a set of polyhedral cells $\{E_i\}$. In this paper we discretize the pressure equation using the two-point flux-approximation (TPFA) method (see e.g., Aziz and Settari 1979). This means that to each interface, say between cell E_i and E_j we associate a (saturation dependent) *transmissibility* t_{ij} which relates the interface flux q_{ij} to the cell-center pressures p_i and p_j through

$$q_{ij} = t_{ij}(p_i - p_j) - G_{ij}. \tag{4}$$

We here let t_{ij} be the harmonic average of the mobility-weighted *half*-transmissibilities, and G_{ij} is the (density-dependent) hydrostatic pressure drop between the corresponding cell-centers.

Using the TPFA, one usually ends up with a system of pressure unknowns, but here, since we will use coarse system bases for the fluxes, we wish to formulate the equations in a system of flux unknowns via a mixed formulation. To derive a mixed discretization of Eq. 2, we let $\boldsymbol{q}$ denote the vector containing the interface fluxes of both interior faces and boundary faces having prescribed pressure boundary conditions (including bottom-hole-pressure constrained wells). Furthermore, let $\boldsymbol{s}$ denote the grid-cell saturations and $\boldsymbol{p}$ the grid-cell pressures. The quantities $\boldsymbol{q}$, $\boldsymbol{p}$ and $\boldsymbol{s}$ are all assumed to be known from the previous time step t^n. The accumulation term in Eq. 2 is then approximated by a backward time-difference. Functional dependencies on pressure are evaluated at the new time step t^{n+1}, whereas dependencies on saturation are evaluated at time t^n. This can be cast in a linearized mixed system of equations which can be solved iteratively. That is, we set $\boldsymbol{q}_0 = \boldsymbol{q}^n$, $\boldsymbol{p}_0 = \boldsymbol{p}^n$, and iteratively solve the linearized, mixed system

$$\begin{bmatrix} \boldsymbol{B}(\boldsymbol{s}_0) & \boldsymbol{C} \\ \boldsymbol{C}^{\mathsf{T}} & \boldsymbol{P}(\boldsymbol{s}_0, \boldsymbol{p}_\nu) \end{bmatrix} \begin{bmatrix} \boldsymbol{q}_{\nu+1} \\ -\boldsymbol{p}_{\nu+1} \end{bmatrix} = \begin{bmatrix} \boldsymbol{f}(\boldsymbol{s}_0, \boldsymbol{p}_\nu) \\ \boldsymbol{g}(\boldsymbol{s}_0, \boldsymbol{p}_0, \boldsymbol{p}_\nu) \end{bmatrix} \tag{5}$$

until $\|\boldsymbol{p}_{\nu+1} - \boldsymbol{p}_\nu\|$ and $\|\boldsymbol{q}_{\nu+1} - \boldsymbol{q}_\nu\|$ are sufficiently small. The matrix $\boldsymbol{P}$ is diagonal with entry $-(c_t|E|/\Delta t)$ for cell E, the matrix $\boldsymbol{B}$ is diagonal with entries t_{ij}^{-1} and $\boldsymbol{C}^{\mathsf{T}}$ is the discrete divergence operator. On the right-hand side of Eq. 5, $\boldsymbol{f}$ contains the inter-cell hydrostatic pressure drops and pressure BCs and $\boldsymbol{g}$ contains the remaining parts of Eq. 2. Assuming compressible fluids in all cells, we can, since $\boldsymbol{P}$ is diagonal eliminate the pressure unknowns to form the system

$$\left(\boldsymbol{B} - \boldsymbol{C}^{\mathsf{T}} \boldsymbol{P}_\nu^{-1} \boldsymbol{C}\right) \boldsymbol{q}_{\nu+1} = \boldsymbol{f}_\nu - \boldsymbol{P}_\nu^{-1} \boldsymbol{g}_\nu, \tag{6}$$

where functional dependencies have been omitted for brevity. When the iteration in Eq. 6 has converged, we set $\boldsymbol{q}^{n+1} = \boldsymbol{q}_{\nu+1}$ and $\boldsymbol{p}^{n+1} = \boldsymbol{p}_{\nu+1}$, and use the updated pressure and total velocity to advance the saturation to time t^{n+1}.

Coarse System Basis

In this section we present a local reduced flux basis for the discretized equation Eq. 6. Let $\{\Omega_i\}_{i=1}^{N_c}$ constitute a coarse grid where each *block* Ω_i contains a connected set of fine grid cells. We will here use three types of coarse-grid bases: the first equal to the (global version of the) MsMFEM basis functions, the second similar to the MsMFEM bases but divergence free, while the third is a coarse grid block-localized POD basis for the remaining span of the snapshots. Assume we have a set of flux-field snapshots $\{\boldsymbol{q}_s\}_{s=1}^{N}$ resulting from one or multiple simulation runs. For each coarse grid interface Γ_{ij}, we perform a singular value decomposition (SVD) of the corresponding fine grid fluxes. Let $\boldsymbol{q}_{s,ij}$ denote the interface fluxes of the s-th snapshot over Γ_{ij} oriented such that the positive direction is from block Ω_i to block Ω_j. Collecting all the vectors $\boldsymbol{q}_{s,ij}$ as columns in a matrix $\boldsymbol{M}_{ij}$, we perform the reduced (thin) SVD such that

$$\begin{aligned}\boldsymbol{M}_{ij} &= \boldsymbol{U}_{ij}\boldsymbol{\Sigma}_{ij}\boldsymbol{V}_{ij}^{\mathsf{T}} \\ &= \sum_{s=1}^{N} \boldsymbol{u}_{s,ij}\sigma_{s,ij}\boldsymbol{v}_{s,ij}^{\mathsf{T}},\end{aligned} \tag{7}$$

with$\boldsymbol{U}_{ij}{}^{\mathsf{T}}\boldsymbol{U}_{ij} = I$, $\boldsymbol{V}_{ij}^{\mathsf{T}}\boldsymbol{V}_{ij} = I$ and $\boldsymbol{\Sigma}_{ij}$ is the diagonal matrix containing the singular values $\sigma_{s,ij}$ in descending order. Letting ϵ be the prescribed tolerance, we truncate the SVD after the first $N_{\epsilon,ij}$ terms where $N_{\epsilon,ij}$ is the smallest number such that $\sum_{s=N_{\epsilon,ij}+1}^{N}\sigma_s < \epsilon$. Accordingly, the first $N_{\epsilon,ij}$ columns of $\boldsymbol{U}_{ij}$ forms a basis for the interface fluxes $\boldsymbol{M}_{ij}$ to prescribed accuracy.

Type 1 : Global version of the MsMFEM basis. The MsMFE basis function $\vec{\psi}_{ij}^{(1)}$ corresponding to an interface Γ_{ij} is composed of the solution of two flow problems such that $\vec{\psi}_{ij}^{(1)} = \vec{\psi}_{i_j} - \vec{\psi}_{j_i}$, where $\vec{\psi}_{k_l}$ is the solution of the incompressible flow problem

$$\vec{\psi}_{k_l} = -\lambda(s_0)\mathbf{K}\nabla p_{k_l}, \qquad \nabla\cdot\vec{\psi}_{k_l} = w_k(x), \tag{8}$$

in Ω_k with

$$\vec{\psi}_{k_l}\cdot\vec{n} = \begin{cases}\vec{u}\cdot\vec{n}, & \text{on } \Gamma_{kl},\\ 0, & \text{on } \partial\Omega_k\setminus\Gamma_{kl},\end{cases} \tag{9}$$

with $\vec{n}$ pointing from Ω_k to Ω_l. In the above equations, s_0 is the initial saturation field (bases are not updated during simulation), and w_k is the basis source function. In this paper we let the basis source function scale according to the porosity, but a constant source would work equally well in this setting although a few more Type 2 and 3 basis functions might be required to span the snapshots to prescribed accuracy. Finally, the normal component of $\vec{u}$ represents the velocity boundary condition (BC).

The MsMFEM basis vector $\boldsymbol{\psi}_{ij}^{(1)}$ is obtained by numerically solving the the discretized version of Eqs. 8 and 9, and by setting the prescribed boundary flux to $\boldsymbol{u}_{1,ij}/\sum\boldsymbol{u}_{1,ij}$, where $\boldsymbol{u}_{1,ij}$ is the first singular vector. A typical MsMFEM basis function is depicted in **Fig. 1**. In principle, one could similarly compute bases for the remaining singular vectors ($\boldsymbol{u}_{2,ij}, ..., \boldsymbol{u}_{N_\epsilon,ij}$), but this may become unstable if the vector has sum close to zero. Instead, we shift the remaining vectors so that they all sum to zero, and then solve a divergence-free flow problem. This produces the Type 2 bases.

Type 2 : Divergence-Free Multiscale Basis. We now construct bases corresponding to the remaining singular vectors $\boldsymbol{u}_2,\ldots,\boldsymbol{u}_{N_{\epsilon,ij}}$. The second type of basis function $\vec{\psi}_{ij}^{(s)}$, $s\geq 2$, corresponding to an interface Γ_{ij} is again composed of the solution to two flow problems such that $\vec{\psi}_{ij}^{(s)} = \vec{\psi}_{i_j} - \vec{\psi}_{j_i}$, where $\vec{\psi}_{k_l}$ is the solution of the incompressible flow problem

$$\vec{\psi}_{k_l} = -\lambda(s_0)\mathbf{K}\nabla p_{k_l}, \qquad \nabla\cdot\vec{\psi}_{k_l} = 0, \tag{10}$$

in Ω_k with

$$\vec{\psi}_{kl}^{\mathrm{h}}\cdot\vec{n} = \begin{cases}\vec{u}\cdot\vec{n}, & \text{on } \Gamma_{kl},\\ 0, & \text{on } \partial\Omega_k\setminus\Gamma_{kl}.\end{cases} \tag{11}$$

We note that the only difference from Eqs. 8 and 9 is the zero source term which requires zero net-flux of $\vec{u}$ across Γ_{ij}. We now obtain the basis vector $\boldsymbol{\psi}_{ij}^{(s)}$ by setting the interface flux to $\boldsymbol{u}_s - \frac{\sum\boldsymbol{u}_s}{\sum\boldsymbol{u}_1}\boldsymbol{u}_1$. This type of basis functions will typically be a rotational field as depicted in **Fig. 1**, although the flow field tends to be more erratic for the singular vectors corresponding to the smaller singular values. The Type 1 and 2 basis vectors now span the flux field snapshots over the coarse grid interfaces to prescribed accuracy, so the remaining snapshot span is localized to the coarse grid blocks interior.

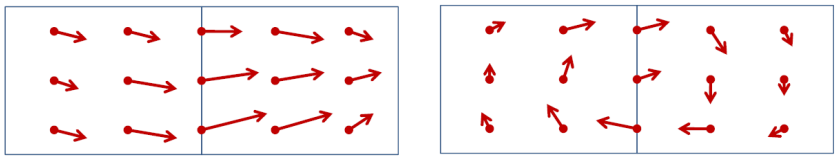

Fig. 1—Standard multiscale (left) and divergence free multiscale (right) basis functions.

Type 3 : Block-Localized POD. The third kind of basis vectors are obtained by truncating one local SVD for each block. Letting $\boldsymbol{q}_{s,i}$ denote the s-th snapshot fluxes in block Ω_i, we perform a SVD such that

$$\boldsymbol{M}_i = \boldsymbol{U}_i \boldsymbol{\Sigma}_i \boldsymbol{V}_i{}^{\mathsf{T}}, \tag{12}$$

where column s of the matrix $\boldsymbol{M}_i$ is given

$$\boldsymbol{M}_i \boldsymbol{e}_s = \boldsymbol{q}_{s,i} - \sum_{\Gamma_{ij} \in \bar{\Omega}_i} \sum_{s=1}^{N_{\epsilon,ij}} \boldsymbol{\psi}_{ij}^{(s)} c_{ij,s}.$$

Here, the coefficients $c_{ij,s}$ ensure that the linear combination of basis functions match (to prescribed tolerance) $\boldsymbol{q}_{s,i}$ over the boundary of the block. The coefficients have in essence already been computed in Eq. 7. As earlier, we now let $N_{\epsilon,i}$ be the smallest number such that $\sum_{s>N_{\epsilon,i}} \sigma_{i,s} < \epsilon$, and define our Type 3 bases simply as $\boldsymbol{\xi}_i^{(s)} = \boldsymbol{u}_{i,s}$, $s = 1, \ldots N_{\epsilon,i}$.

By construction, the bases $\{\boldsymbol{\psi}_{ij}^{(s)}\}$ and $\{\boldsymbol{\xi}_i^{(s)}\}$ span the snapshot space to prescribed accuracy. Collecting the bases as columns in matrices $\boldsymbol{\Psi}$ and $\boldsymbol{\Xi}$, respectively, the reduced version of Eq. 6 becomes

$$[\boldsymbol{\Psi}\ \boldsymbol{\Xi}]^{\mathsf{T}} \left(\boldsymbol{B} - \boldsymbol{C}^{\mathsf{T}} \boldsymbol{P}_\nu^{-1} \boldsymbol{C}\right) [\boldsymbol{\Psi}\ \boldsymbol{\Xi}]\, \boldsymbol{q}_{\nu+1,c} = [\boldsymbol{\Psi}\ \boldsymbol{\Xi}]^{\mathsf{T}} \left(\boldsymbol{f}_\nu - \boldsymbol{P}_\nu^{-1} \boldsymbol{g}_\nu\right), \tag{13}$$

with $\boldsymbol{q}_{\nu+1} = [\boldsymbol{\Psi}\ \boldsymbol{\Xi}]\, \boldsymbol{q}_{\nu+1,c}$. We note that after solving Eq. 13, the coarse-grid fluxes and divergence are dictated by the MsMFEM basis functions $\{\boldsymbol{\psi}_{ij}^{(1)}\}$, since $\{\boldsymbol{\psi}_{ij}^{(s)}\}$, $s \geq 2$, and $\{\boldsymbol{\xi}_i^{(s)}\}$ all have zero coarse grid means. Finally, we note that the system Eq. 13 can be further reduced. Due to the localized nature of the block-localized POD bases (Type 3), we have that

$$\boldsymbol{\xi}_i^{(s_1)^{\mathsf{T}}} \left(\boldsymbol{B} - \boldsymbol{C}^{\mathsf{T}} \boldsymbol{P}_\nu^{-1} \boldsymbol{C}\right) \boldsymbol{\xi}_j^{(s_2)} = 0, \quad i \neq j.$$

It follows that $\boldsymbol{\Xi}^{\mathsf{T}} \left(\boldsymbol{B} - \boldsymbol{C}^{\mathsf{T}} \boldsymbol{P}_\nu^{-1} \boldsymbol{C}\right) \boldsymbol{\Xi}$ is block diagonal, and that (provided the matrix blocks are not too large) the corresponding unknowns can efficiently be eliminated from the system via a Schur complement procedure.

Numerical Examples

We now present numerical experiments using the reduced basis outlined in the previous section. Both experiments construct the bases using a single tuning simulation, and the overall process can be described in the following steps:

1. One tuning simulation is performed, and several flux-field snapshots are saved to disk.
2. A coarse grid is constructed, and coarse grid interface fluxes are collected from the snapshots.
3. We compute the truncated SVDs of the interface flux distributions.
4. For each block we collect all corresponding interface BCs, and solve one linear system with multiple right-hand-sides to produce the Type 1 and 2 basis functions.
5. For each block we subtract the linear combination of Type 1 and 2 basis functions from the snapshots producing zero flux over the block boundary, and compute the truncated SVD of the remaining flux fields to produce the Type 3 bases.
6. The configuration of the tuning simulation is changed, and the corresponding simulation is performed using the reduced bases.
7. Finally, we run a full (fine grid) simulation with the new configuration for reference.

A short comment to point 4 in the above list is in order; typically, the linear systems arising in the computation of basis functions are small to medium and efficiently solved using direct methods for sparse linear systems (see e.g, Davis (2006)). Such methods based on sparse LU-decompositions are particularly efficient for systems with multiple right-hand-sides, and in our experience the difference in computational time for solving a linear system with a singe right-hand-side to a system with a few tens of right-hand-sides is insignificant. It follows that even if the number of basis functions become large, the time it takes to compute them can be kept low.

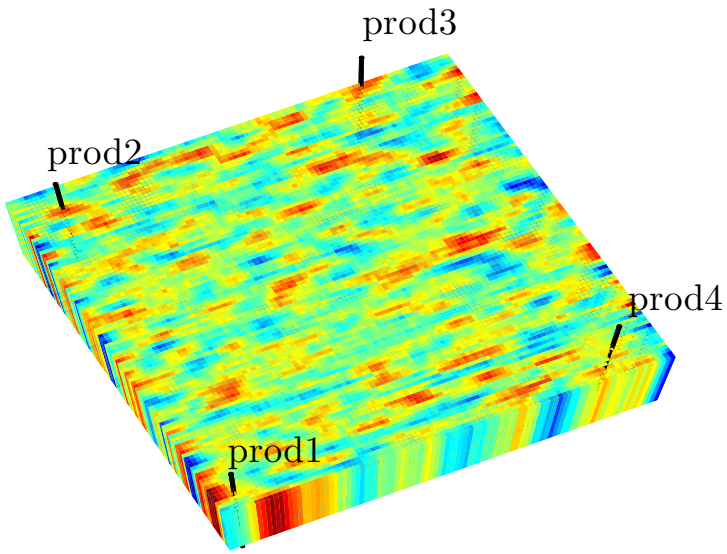

Fig. 2—Model for Example 1 displaying a log-normally distributed permeability field and the four production wells.

TABLE 1—Results for various reduced models in Example 1, number of basis functions and basis storage requirements (double precision).

Dims	Error	# Facebases	# Blockbases	Stoarge
2×2	6.9×10^{-2}	9	30	4.8 Mb
4×4	9.5×10^{-3}	36	42	2.9 Mb
8×8	2.3×10^{-3}	139	73	2.2 Mb
16×16	1.3×10^{-3}	540	132	1.9 Mb
25×25	9.2×10^{-4}	1299	184	1.9 Mb

Example 1 : Primary Production From a Gas Reservoir. In this experiment we consider a 2D reservoir initially filled with gas at 400 bars. Four wells (see **Fig. 2**) start producing simultaneously; Prod1 and Prod3 at 80 bars and Prod2 and Prod4 at 130 bars. The tuning run produces 80 snapshots more which are more densely distributed at early simulation times. Reduced bases for several coarse grids are computed based on these snapshots with a relative tolerance of 10^{-3}. After the tuning-run, and computation of bases, the configuration is changed such that Prod1 and Prod3 now produce at 130 bars and Prod2 and Prod4 at 80 bars. The producer well rates for the tuning-run and subsequent reference-run are depicted in **Fig. 3** showing apparent differences. Reduced bases were computing for coarse grids of dimensions 1×1, 2×2, 4×4, 8×8, 16×16 and 25×25. The reduced model based on the 1×1 coarse grid did not converge, so only results from the remaining grids are reported. We measure the performance of the reduced models by comparing the well rates. That is, for each reduced model run, we compute maximal individual well rate misfit over the total simulation time between the reduced model run and the reference run. The results are reported in **Table 1**. As can be seen, all reduced models from 4×4 and finer, produce well rates within 1% error. In columns 3 and 4 the number of coarse model face bases (Type 1 and 2) and block bases (Type 3) are reported. Recall that the unknowns corresponding to the Type 3 bases can be eliminated from the coarse systems as long as the number of basis vectors for each block is not too large. Obviously, finer coarse grids require higher dimensional bases, but increasing the coarse grid resolution also increases the bases sparsity. This is illustrated in column 5 where we have reported the storage requirements (double precision) for the bases. In this example, the complexity of the flow is largest in the near-well regions, and this is reflected in the number of required local basis vectors. In **Fig. 4** we have plotted the number of Type 3 bases required for the coarse grid cases 8×8 and 16×16. Observe that furthest away from the wells, no block bases are required.

Example 2: A Vertical Slice With Strong Gravitational Effects. In this experiment we consider a 2D vertical slice of a reservoir (see **Fig. 5**) initially filled with compressible oil at 150 bars. We place an injector at the left (perforating all 20 cells), and similarly a producer at the right. In the tuning run, we inject gas at a constant BHP of 300 bars, while the producer is set to produce at 80 bars. This induces a flowing rate sufficiently small so that gravity plays an important role. During the tuning-run, we save 100 snapshots. Reduced bases were computed for coarse grids of dimensions 1×1, 5×1, 10×2, 10×5, 10×10 and 20×10 with a relative tolerance of 10^{-3}. For the reference run, we decrease the injector BHP to 250 bars. In **Fig. 6** we have compared the saturation profiles for the tuning and reference run just after gas breakthrough (but at different times). As can bee seen, for the tuning run, the gas breakthrough appears in the lower middle part of the producer, while for the slower flowing

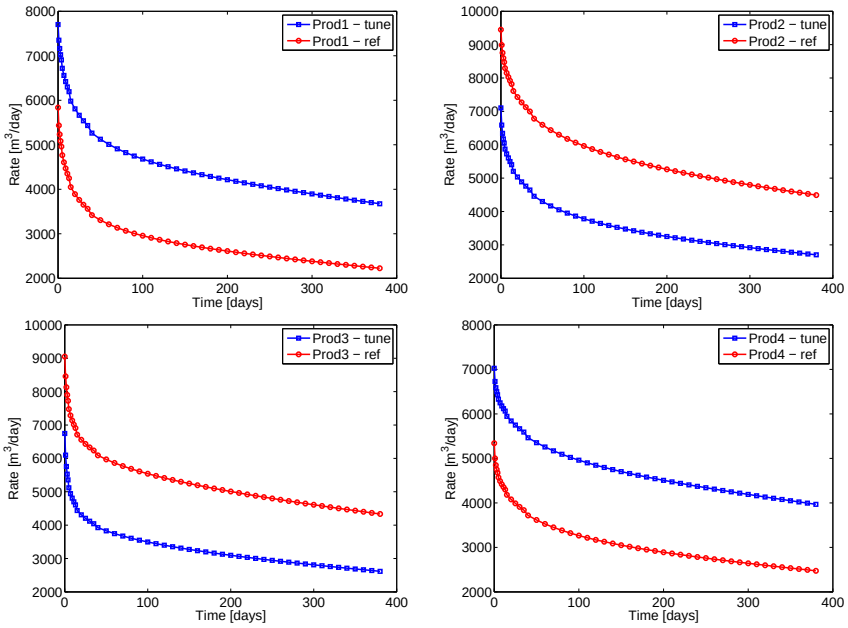

Fig. 3—Well production rates for both the tuning-run and the reference-run Example 1.

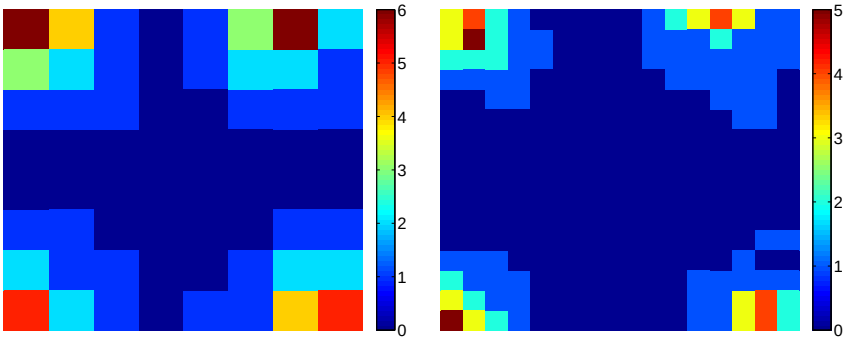

Fig. 4—Number of Type 3 bases for blocks in coarse grids 8×8 (left) and 16×16 (right).

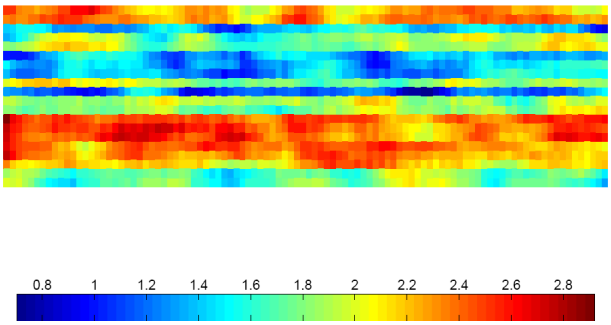

Fig. 5—Model for Example 2 displaying a log-normally distributed layered permeability field

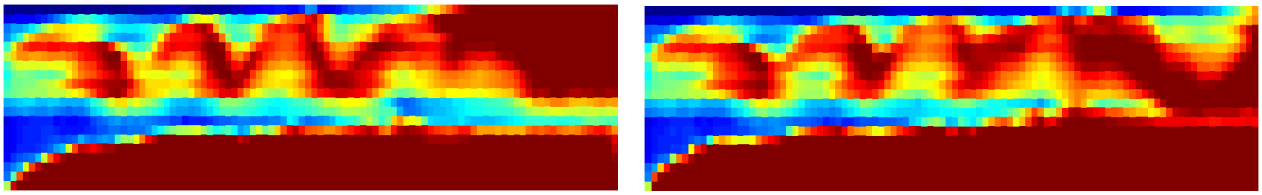

Fig. 6—Gas saturation profile for the tuning run (left) and the reference run (right) just after gas breakthrough.

reference run, the breakthrough appears in the top layer. Again, the 1×1 coarse model failed to produce a result and is not reported. For the remaining reduced models, we measure the gas saturation error compared to the reference at 685 days which is just after gas breakthrough. We use the error measure

$$e_s(s_g) = \frac{\int_\Omega |s_g^{\text{ref}} - s_g|}{\int_\Omega s_g^{\text{ref}}}.$$

The results are reported in **Table 2**, and it is clear that vertical coarse grid resolution is needed for the bases to capture the reference case accurately. It is also clear that this example constitutes a much more complex flow than the first example regarding the high number of required basis vectors. Again, we observe that the bases storage requirements decrease with increasing resolution. For visual comparison, we have in **Fig. 7** depicted the corresponding saturation profiles for the three reduced models based on the coarsest grids (the remaining two match the reference closely and are not plotted). It is clear that the model based on the 5×1-grid fails; in fact the saturation profile much more resembles the tuning-run profile for the given time. Increasing the resolution to 10×2 improves the result significantly. Local variations in the number of required basis vectors is observed also in this model. In **Fig. 8** we have depicted the number of required block bases (Type 3) for the 10×5 and 10×10 cases. We see that a large number of basis vectors are needed around the wells and along the fluid interfaces. The total amount of basis functions required in this example suggests that finding efficient low order models for such problems are difficult without sacrificing accuracy. If only a part of the reservoir is gravity dominated, however, the approach will naturally adapt and the procedure can still be efficient.

Concluding Remarks

We have presented a coarse grid localized model order reduction methodology based on MsMFEM basis functions and local PODs for coarse grid interface fluxes and coarse grid-block interior fluxes. Except for the reduced models based on very coarse grids, the strategy produced results matching closely the reference for the cases considered, even for a reference considerably different from the tuning run. The choice of coarse grid resolution appear to have the following effects: a very coarse grid requires few basis functions but is less process independent and requires more storage, a fine coarse grid requires more basis functions

TABLE 2—Results for various reduced models in Example 2, number of basis functions and basis storage requirements (double precision).

Dims	Error	# Facebases	# Blockbases	Stoarge
5×1	0.396	55	195	5.1 Mb
10×2	0.134	171	424	3.3 Mb
10×5	0.053	387	535	2.2 Mb
10×10	0.038	694	624	1.7 Mb
20×10	0.037	908	585	1.0 Mb

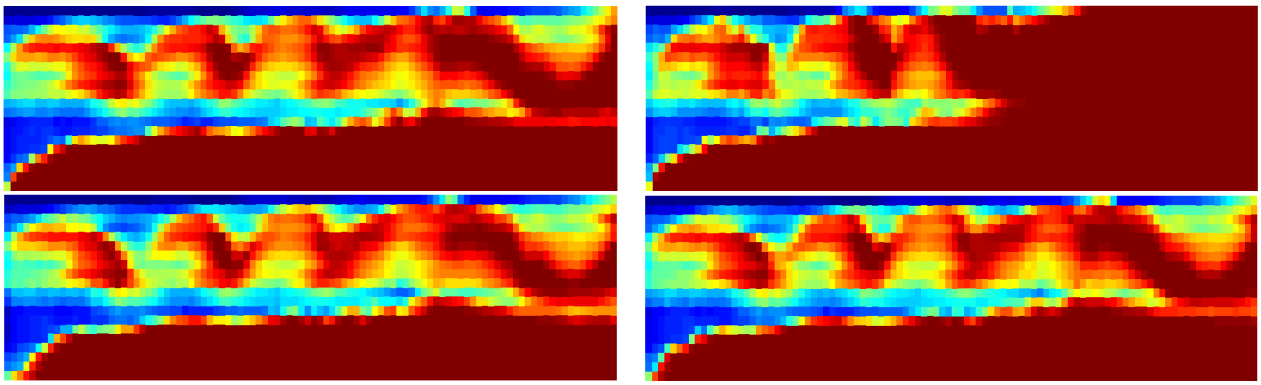

Fig. 7—Gas saturation profile for the reference run (top left), reduced model run 5×1 (top right), reduced model run 10×2 (bottom left) and reduced model run 10×5 (bottom right).

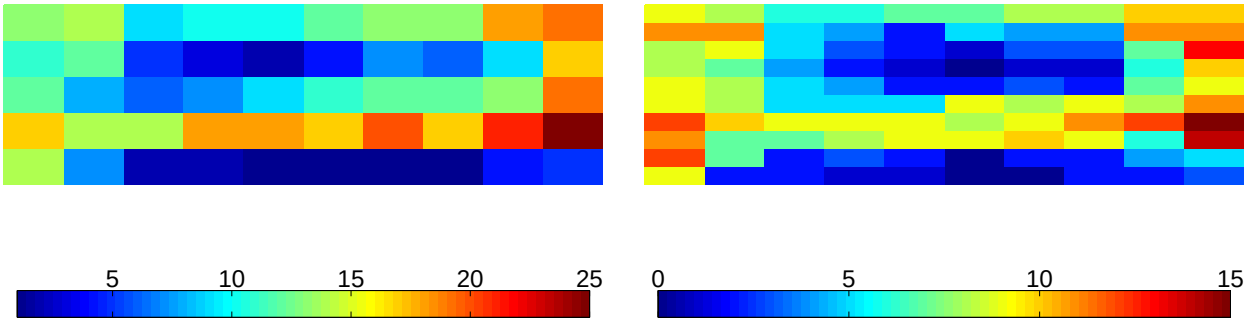

Fig. 8—Number of block bases required in reduced models based on grids 10×5 (left) and 10×10 (right).

but is more process independent and requires less storage. As a result, the optimal strategy is somewhere in between the two extremes.

Acknowledgements

The author gratefully acknowledge financial support by the Center for Intgrated Operations in the Petroleum Industry at NTNU.

Nomenclature

Physical quantities:

$\mathbf{K}$	=	absolute permeability
p	=	pressure
s	=	saturation
t	=	time
q	=	volumetric rate
$\vec{u}$	=	total Darcy velocity
λ	=	total mobility
ϕ	=	porosity

Domain and grid:

Ω	=	entire physical domain
∂D	=	boundary of domain D
E	=	cell in the fine grid
Ω_i	=	coarse block number i
Γ_{ij}	=	interface between block number i and j

Functions, etc:

$\vec{\psi}_{ij}^{(s)}$	=	s-th basis function for interface between block i and j
$\vec{\psi}_{i_j}$	=	basis function localized to block i
w_i	=	weight function associated with coarse block Ω_i

Vectors and matrices:

$\boldsymbol{s}$	=	vector of cell saturations
$\boldsymbol{p}$	=	vector of cell pressures
$\boldsymbol{q}$	=	vector of face fluxes
$\boldsymbol{\psi}_{ij}^{(s)}$	=	basis vector (discrete version of $\vec{\psi}_{ij}^{(s)}$)
$\boldsymbol{\xi}_i^{(s)}$	=	s-th basis vector for block i
$\boldsymbol{\Psi}$	=	matrix of all interface basis vectors
$\boldsymbol{\Xi}$	=	matrix of all block basis vectors

Subscripts:

i, j	=	block/cell numbers
n	=	time step
s	=	referring to snapshot or term in SVD

References

Aarnes, J., Efendiev, Y., and Jiang, L. 2008. Mixed Multiscale Finite Element Methods Using Limited Global Information. *Multiscale Model. Simul.*, 7(2):655–676.

Aarnes, J. E., Krogstad, S., and Lie, K.-A. 2006. A Hierarchical Multiscale Method for Two-Phase Flow Based Upon Mixed Finite Elements and Nonuniform Coarse Grids. *Multiscale Model. Simul.*, 5(2):337–363 (electronic).

Aziz, K. and Settari, A. 1979. *Petroleum Reservoir Simulation*. Elsevier Applied Science Publishers, London and New York.

Cardoso, M. A., Durlofsky, L. J., and Sarma, P. 2008. Development and Application of Reduced-Order Modeling Procedures for Subsurface Flow Simulation. *Int. J. Numer. Meth. Eng.*, 77(9):1322–1350.

Davis, T. A. 2006. *Direct Methods for Sparse Linear Systems*. Fundamentals of Algorithms. Society for Industrial and Applied Mathematics, Philadelphia, PA, USA.

Effendiev, Y., Ginting, V., Hou, T., and Ewing, R. 2006. Accurate Multiscale Finite Element methods for two-phase flow simulations. *J. Comput. Phys.*, 220(1):155–174.

Krogstad, S., Lie, K.-A., Nilsen, H. M., Natvig, J. R., Skaflestad, B., and Aarnes, J. E. 2009. A Multiscale Mixed Finite-Element Solver for Three-Phase Black-Oil Flow. Paper SPE 118993, presented at SPE Reservoir Simulation Symposium, The Woodlands, TX, USA, 2–4 February.

Lunati, I. and Jenny, P. 2006. Multiscale Finite-Volume Method for Compressible Multiphase Flow in Porous Media. *J. Comput. Phys.*, 216(2):616–636.

Skaflestad, B. and Krogstad, S. 2008. Multiscale/Mimetic Pressure Solvers With Near-Well Grid Adaption. In *Proceedings of ECMOR XI–11th European Conference on the Mathematics of Oil Recovery*, number A36, Bergen, Norway. EAGE.

Tchelepi, H., Jenny, P., Lee, S., and Wolfsteiner, C. 2007. Adaptive Multiscale Finite Volume Framework for Reservoir Simulation. *SPE J.*, 12:188–195. Doi: 10.2118/93395-PA.

van Doren, J. F. M., Markovinovic, R., and Jansen, J. D. 2006. Reduced-Order Optimal Control of Water Flooding Using Proper Orthogonal Decomposition. *Comput. Geosci.*, 10(1):137–158.